# Supplementary Materials

## *In Vitro* Screening of Anti-Viral and Virucidal Effects Against SARS-Cov-2 by Phenylamino-Phenoxy-Quinoline Derivatives: An Integrative Computational Approach

**Suwicha Patnin[1], Arthit Makarasen[1]*, Akanitt Jittmittraphap[2], Pornsawan Leaungwutiwong[2], Pongsit Vijitphan[1], Apisara Baicharoen[1], Natchaphon Ngueanngam[3] and Supanna Techasakul[1]***

[1] Department of Chemistry, Laboratory of Organic Synthesis, Chulabhorn Research Institute, Bangkok 10210, Thailand

[2] Department of Microbiology and Immunology, Faculty of Tropical Medicine, Mahidol University, Bangkok 10400, Thailand

[3] Department of Chemistry, Faculty of Science, Srinakharinwirot University, Bangkok 10110, Thailand

*Correspondence: arthit@cri.or.th, supanna@cri.or.th

These figures depict the two-dimensional binding mode and intricate binding interactions taking place in the active site of the Main Protease ($M^{pro}$). The results of molecular docking showcase the binding interactions of quinoline derivatives **1(a-d)**, **2(a-d)**, and **3(a-d)**, in addition to commercially accessible medications (ritonavir, ensitrevir, and nirmatrelvir). The analysis of these interactions is conducted within the binding pocket, defined within a radius of 3.0 Å from $M^{pro}$, as detailed below.

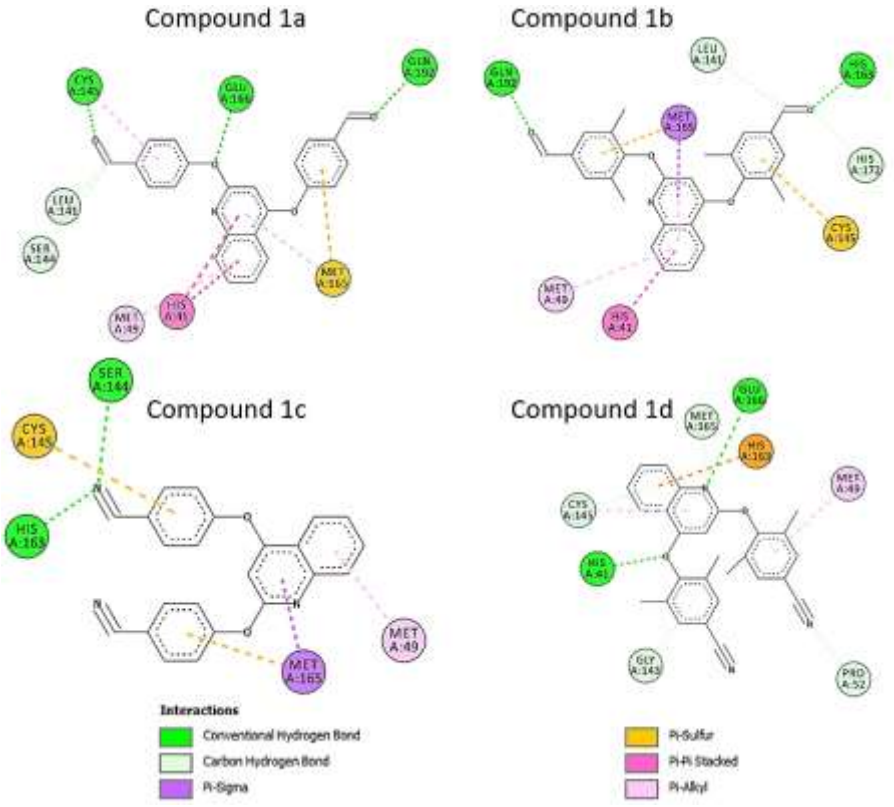


**Figure S1** 2-dimensional interaction diagram between compound **1(a-d)** and $M^{pro}$.

For **2,4-di-(4′-formylphenoxy)-quinoline (1a)**, the amino acid residues of $M^{pro}$ within a 5.0 Å radius included HIS41, MET49, PRO52, TYR54, CYS145, HIS164, MET165, GLU166, LEU167, PRO168, ASP187, ARG188, GLN189, THR190, and GLN192. The conventional hydrogen bonding interactions between $M^{pro}$ and **1a** were observed, such as those between the H atom of the $NH_2$ group in CYS145 and the O atom of the C=O group in **1a**, between the H atom of the $NH_2$ group in GLN192 and the O atom of the C=O group in **1a**, and between the H atom of the $NH_2$ group in GLU166 and the O atom of **1a**. Additionally, three carbon hydrogen bonds were formed with LEU141, SER144, and ALA191, and one π-Sulfur interaction was displayed with MET165, and one π-Alkyl interaction was observed with MET49. In addition, one hydrophobic interaction was performed using π-π stacking between HIS41 and **1a**.

For **2,4-di-(2′,6′-Dimethyl-4′-formylphenoxy)-quinoline (1b)**, the amino acid residues of $M^{pro}$ within a 5.0 Å radius included HIS41, MET49, PRO52, TYR54, CYS145, HIS164, MET165, GLU166, LEU167, PRO168, ASP187, ARG188, GLN189, THR190, and GLN192. The conventional hydrogen bonding interactions between $M^{pro}$ and **1b** were demonstrated, such as those between the H atom of the $NH_2$ group in HIS163 and the O atom of the C=O group in **1b**, and between the H atom of the $NH_2$ group in GLN192 and the O atom of the C=O group in **1b**. Two carbon hydrogen bonds were formed with LEU141 and HIS172, one π-Sulfur interaction was observed with CYS145, and one π-Alkyl interaction was observed with MET49. In addition, one hydrophobic interaction was performed using π-π stacking between HIS41 and **1b**.

For **2,4-di-(4′-cyanophenoxy)-quinoline (1c)**, the amino acid residues of $M^{pro}$ within a 5.0 Å radius included HIS41, MET49, PRO52, TYR54, CYS145, HIS164, MET165, GLU166, LEU167, PRO168, ASP187, ARG188, GLN189, THR190, and GLN192. The conventional hydrogen bonding interactions between $M^{pro}$ and **1c** were observed, such as those between the H atom of the OH group in SER144 and the N atom of the CN group in **1c** and between the H atom of the $NH_2$ group in HIS163 and the N atom of the CN group in **1c**. Moreover, two π-Sulfur interactions were displayed with CYS145 and MET165, and one π-Alkyl interaction was observed with MET49.

For **2,4-di-(2′,6′-Dimethyl-4′-cyanophenoxy)-quinoline (1d)**, the amino acid residues of $M^{pro}$ within a 5.0 Å radius included HIS41, MET49, PRO52, TYR54, CYS145, HIS164, MET165, GLU166, LEU167, PRO168, ASP187, ARG188, GLN189, THR190, and GLN192. The conventional hydrogen bonding interactions between $M^{pro}$ and **1d** were demonstrated, such as those between the H atom of the $NH_2$ group in HIS41 and the N atom of **1d** and between the H atom of the $NH_2$ group in GLU166 and the O atom of **1d**. Two carbon hydrogen bonds were formed with PRO52 and MET165, two π-Donor hydrogen bond interactions were observed with GLY143, CYS145, and one π-Alkyl interaction was observed with MET49.

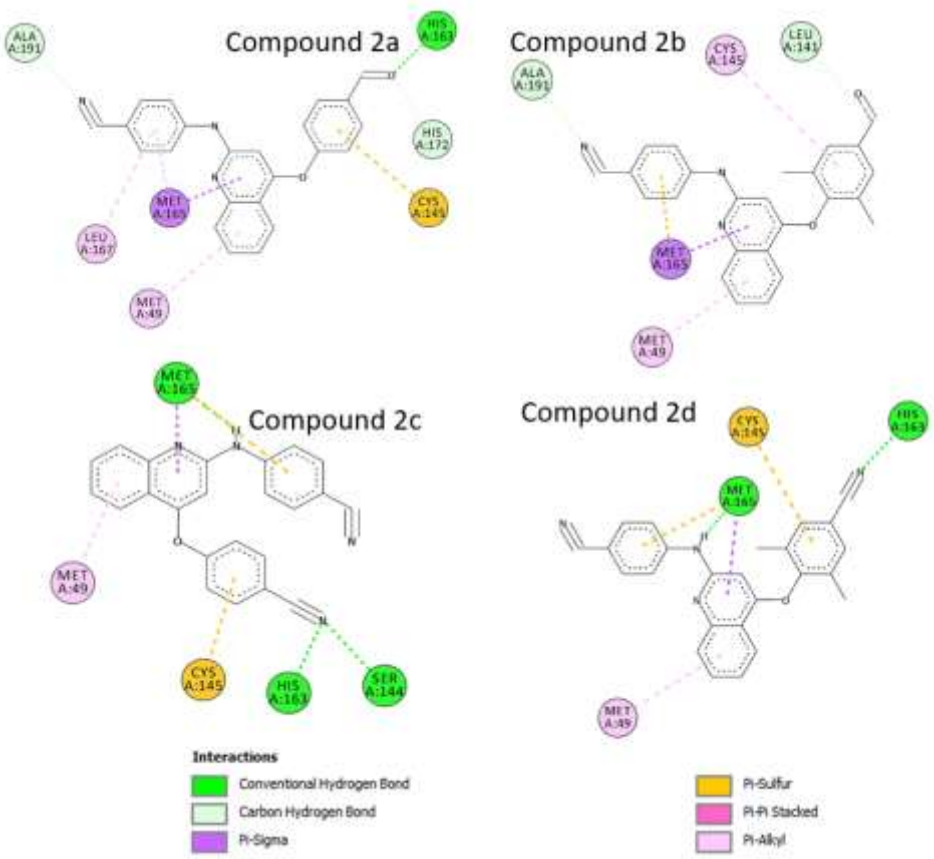


**Figure S2** 2-dimensional interaction diagram between compound **2(a-d)** and $M^{pro}$.

For **4-(4′-formylphenoxy)-2-(4″-cyanophenyl)-aminoquinoline (2a)**, the amino acid residues of $M^{pro}$ within a 5.0 Å radius included HIS41, MET49, PRO52, TYR54, CYS145, HIS164, MET165, GLU166, LEU167, PRO168, ASP187, ARG188, GLN189, THR190, and GLN192. The conventional hydrogen bonding interactions between $M^{pro}$ and **2a** were observed, such as those between the H atom of the $NH_2$ group in HIS163 and the O atom of the C=O group in **2a**. Two carbon hydrogen bonds were formed with HIS172 and ALA191, and one π-Sulfur interaction was displayed with CYS145, along with two π-Alkyl interactions observed with MET49 and LEU167.

For **4-(2′,6′-Dimethyl-4′-formylphenoxy)-2-(4″-cyanophenyl)-aminoquinoline (2b)**, the amino acid residues of $M^{pro}$ within a 5.0 Å radius included HIS41, MET49, PRO52, TYR54, CYS145, HIS164, MET165, GLU166, LEU167, PRO168, ASP187, ARG188, GLN189, THR190, and GLN192. Two carbon hydrogen bonds were formed with LEU141 and ALA191, one π-Sulfur interaction was observed with MET165, and two π-Alkyl interactions were observed with MET49 and CYS145.

For **4-(4′-cyanophenoxy)-2-(4″-cyanophenyl)-aminoquinoline (2c)**, the amino acid residues of $M^{pro}$ within a 5.0 Å radius included HIS41, MET49, PRO52, TYR54, CYS145, HIS164, MET165, GLU166, LEU167, PRO168, ASP187, ARG188, GLN189, THR190, and GLN192. The conventional hydrogen bonding interactions between $M^{pro}$ and 5c were observed, such as those between the H atom of the OH group in SER144 and the N atom of the CN group in **2c**, between the H atom of the $NH_2$ group in HIS163 and the N atom of the CN group in **2c**, and those between the S atom of the SH group

in MET165 and the H atom of the $NH_2$ group in **2c**. Moreover, one π-Sulfur interaction was displayed with CYS145, and one π-Alkyl interaction was observed with MET49.

For **4-(2′,6′-Dimethyl-4′-cyanophenoxy)-2-(4″-cyanophenyl)-aminoquinoline (2d)**, the amino acid residues of $M^{pro}$ within a 5.0 Å radius included HIS41, MET49, PRO52, TYR54, CYS145, HIS164, MET165, GLU166, LEU167, PRO168, ASP187, ARG188, GLN189, THR190, and GLN192. The conventional hydrogen bonding interactions between $M^{pro}$ and **2d** were demonstrated, such as those between the H atom of the $NH_2$ group in HIS163 and the N atom of the CN group in **2d** and those between the S atom of the SH group in MET165 and the H atom of the $NH_2$ group in **2d**. Two π-Sulfur interactions were observed with CYS145, MET165, and one π-Alkyl interaction was observed with MET49.

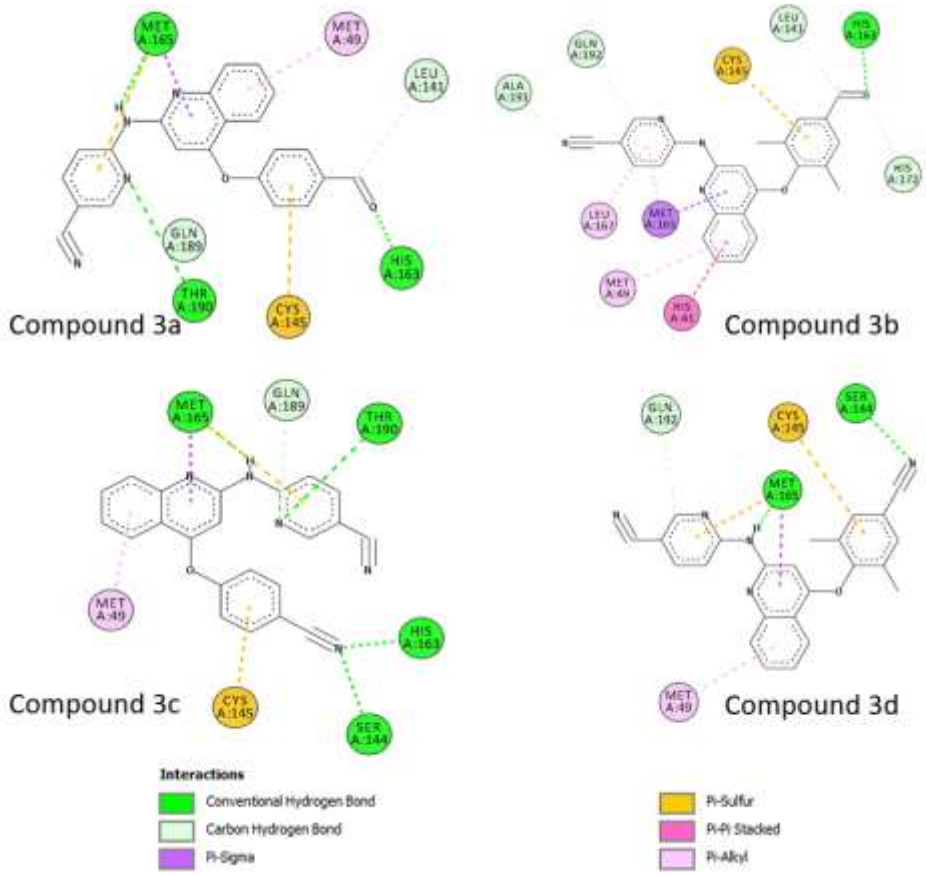


**Figure S3** 2-dimensional interaction diagram between compound **3(a-d)** and $M^{pro}$.

For **4-(4'-formylphenoxy)-2-(5″-cyanopyridin-2″ylamino)quinoline (3a)**, the amino acid residues of $M^{pro}$ within a 5.0 Å radius included HIS41, MET49, PRO52, TYR54, CYS145, HIS164, MET165, GLU166, LEU167, PRO168, ASP187, ARG188, GLN189, THR190, and GLN192. The conventional hydrogen bonding interactions between $M^{pro}$ and **3a** were observed, such as those between the H atom of the $NH_2$ group in HIS163 and the O atom of the C=O group in **3a**, between the S atom of the SH group in MET165 and the H atom of the $NH_2$ group in **3a**, and between the H atom of the $NH_2$ group in THR190 and the N atom of the $NH_2$ group in **3a**. Additionally, two carbon hydrogen

bonds were formed with LEU141 and GLN189, and interactions included one π-Sulfur interaction with CYS145 and one π-Alkyl interaction with MET49.

For **4-(2′,6′-Dimethyl-4′-formylphenoxy)-2-(5′′-cyanopyridin-2′′ylamino)quinoline (3b)**, the amino acid residues of $M^{pro}$ within a 5.0 Å radius included HIS41, MET49, PRO52, TYR54, CYS145, HIS164, MET165, GLU166, LEU167, PRO168, ASP187, ARG188, GLN189, THR190, and GLN192. The conventional hydrogen bonding interactions between $M^{pro}$ and **3b** were observed, such as those between the H atom of the $NH_2$ group in HIS163 and the O atom of the C=O group in **3b**. In addition, four carbon hydrogen bonds were formed with LEU141, HIS172, ALA191, and GLN192, and interactions included one π-Sulfur interaction with CYS145 and two π-Alkyl interactions with MET49 and LEU167. Furthermore, a π- π stacking interaction between the HIS41 residue and the benzene ring of **3b** was observed.

For **4-(4′-cyanophenoxy)-2-(5′′-cyanopyridin-2′′ylamino)quinoline (3c)**, the amino acid residues of $M^{pro}$ within a 5.0 Å radius included HIS41, MET49, PRO52, TYR54, CYS145, HIS164, MET165, GLU166, LEU167, PRO168, ASP187, ARG188, GLN189, THR190, and GLN192. The conventional hydrogen bonding interactions between $M^{pro}$ and **3c** were observed, such as those between the H atom of the OH group in SER144 and the N atom of the CN group in **3c**, between the H atom of the $NH_2$ group in HIS163 and the N atom of the CN group in **3c**, between the S atom of the SH group in MET165 and the H atom of the $NH_2$ group in **6c**, and those between the H atom of the $NH_2$ group in THR190 and the N atom of the $NH_2$ group in **3c**. Additionally, one carbon hydrogen bond was formed with GLN189. Moreover, one π-Sulfur interaction was displayed with CYS145, and one π-Alkyl interaction was observed with MET49.

For **4-(2′,6′-Dimethyl-4′-cyanophenoxy)-2-(5”-cyanopyridin-2”ylamino)quinoline (3d)**, the amino acid residues of $M^{pro}$ within a 5.0 Å radius included HIS41, MET49, PRO52, TYR54, CYS145, HIS164, MET165, GLU166, LEU167, PRO168, ASP187, ARG188, GLN189, THR190, and GLN192. The conventional hydrogen bonding interactions between $M^{pro}$ and **3d** were established, such as those involving the H atom of the $NH_2$ group in SER144 and the N atom of the CN group in **3d**, and those connecting the S atom of the SH group in MET165 with the H atom of the $NH_2$ group in **3d**. Additionally, one carbon hydrogen bond formed with GLN192. Two π-Sulfur interactions were interacted with CYS145 and MET165, and one π-Alkyl interaction occurred with MET49.

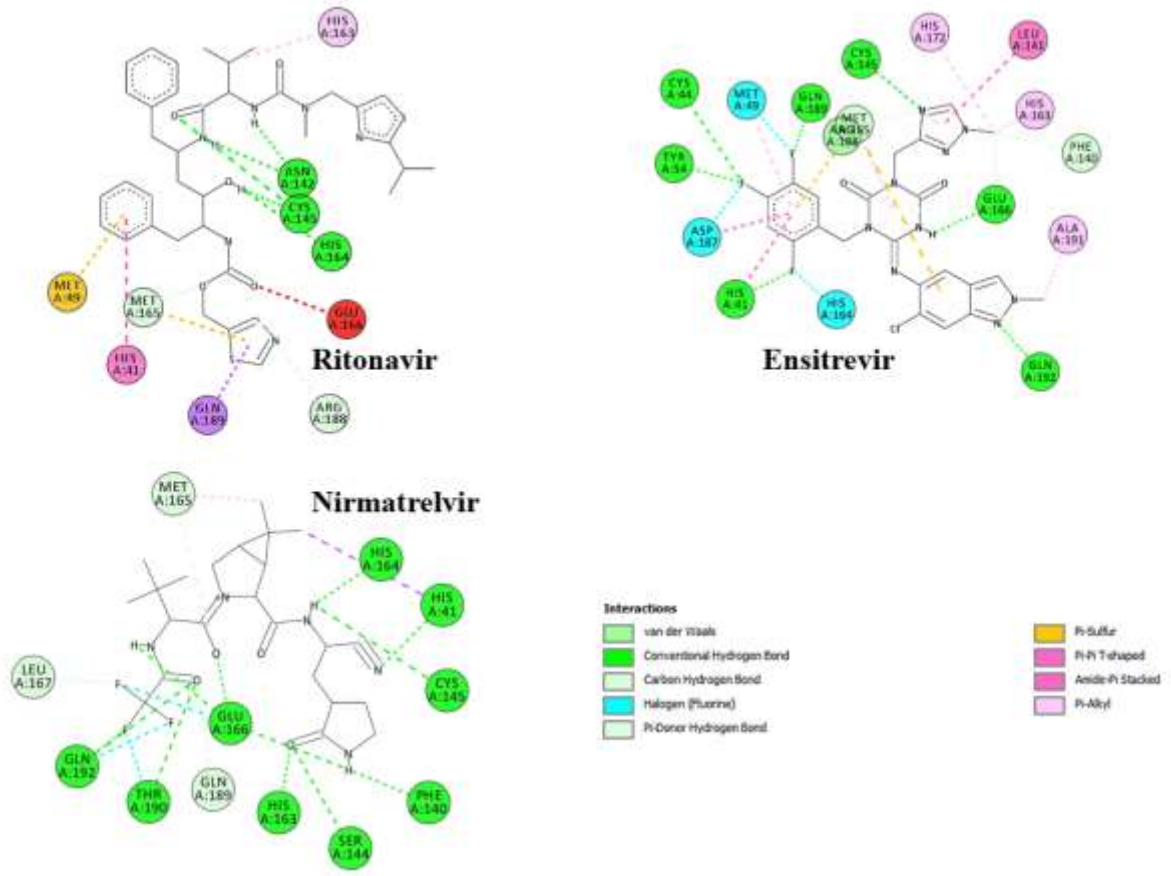


**Figure S4** 2-dimensional interaction diagram between commercially accessible medications and $M^{pro}$.

For ritonavir, the amino acid residues of $M^{pro}$ within 5.0 Å included HIS41, MET49, TYR54, PHE140, LEU141, ASN142, GLY143, SER144, CYS145, HIS163, HIS164, MET165, GLU166, LEU167, PRO168, ASP187, ARG188, and GLN189. The conventional hydrogen bonding interactions between $M^{pro}$ and ritonavir were observed, such as those between the O-atom of the C=O group in ASN142 and the H-atom of the $NH_2$ group in ritonavir, between the S atom of the SH group in CYS145 and the H atom of OH group in ritonavir, between the O atom of the C=O group in HIS164 and the H atom of OH group in ritonavir. Two carbon hydrogen bonds were formed with MET165, ARG188 and one π-Donor interaction was displayed with GLU166. Furthermore, a π-π stacking interaction was noted between the HIS41 residue and the benzene ring of ritonavir.

For ensitrevir, the amino acid residues of $M^{pro}$ within a 5.0 Å radius surrounding ensitrevir included HIS41, MET49, TYR54, PHE140, LEU141, GLY143, SER144, CYS145, HIS163, HIS164, MET165, GLU166, HIS172, and ARG188. The conventional hydrogen bonding interactions between $M^{pro}$ and ensitrevir were demonstrated, such as those between the H atom of the $NH_2$ group in HIS41 and the F atom of the benzyl group in ensitrevir, between the H atom of the OH group in TYR54 and the F atom of the benzyl group in ensitrevir, between the H atom of the SH group in CYS145 and the N atom of the $NH_2$ group in ensitrevir, between the O atom of the C=O group in GLU166 and the H atom of the $NH_2$ group in ensitrevir, between the H atom of the $NH_2$ group in GLN192 and the N atom

of ensitrevir, and between the H atom of the $NH_2$ group in GLN189 and the F atom of the benzyl group in ensitrevir. Three carbon hydrogen bonds interacted with PHE140, MET165, and GLU166, and one π-donor hydrogen bond was formed with GLU166. Additionally, one π-Sulfur interaction occurred with MET165, and two π-Alkyl interactions were observed with HIS163 and HIS172. A π-π stacking interaction between the HIS41 residue of $M^{pro}$ and the benzene ring of ensitrevir was also observed.

For nirmatrelvir, the amino acid residues of $M^{pro}$ within a 5.0 Å radius included HIS41, MET49, PRO52, TYR54, HIS163, HIS164, MET165, GLU166, PRO168, ARG188, THR190, ALA191, and GLN192. Nirmatrelvir demonstrated the conventional hydrogen bonding interactions with $M^{pro}$. These included interactions between the H atom of the $NH_2$ group in HIS41 and the N atom of the CN group in nirmatrelvir, the N atom of the $NH_2$ group in PHE140 and the H atom of the $NH_2$ group in nirmatrelvir, the H atom of the OH group in SER144 and the O atom of the C=O group in nirmatrelvir, the H atom of the SH group in CYS145 and the N atom of the $NH_2$ group in nirmatrelvir, the H atom of the $NH_2$ group in HIS163 and the O atom of the C=O group in nirmatrelvir, the O atom of the C=O group in HIS164 and the H atom of the $NH_2$ group in nirmatrelvir, the N atom of the $NH_2$ group in THR190 and the O atom of the C=O group in nirmatrelvir, and the N atom of the $NH_2$ group in GLN192 and the O atom of the C=O group in nirmatrelvir. Additionally, three conventional hydrogen bonding interactions formed between the O atom of the C=O group in GLU166 and the H atom of the $NH_2$ group in nirmatrelvir, between the O atom of the C=O group in GLU166 and the H atom of the $NH_2$ group in nirmatrelvir, and between the N atom of the $NH_2$ group in GLU166 and the O atom of the C=O group in nirmatrelvir. Two carbon hydrogen bonds were displayed with MET165 and GLN189.

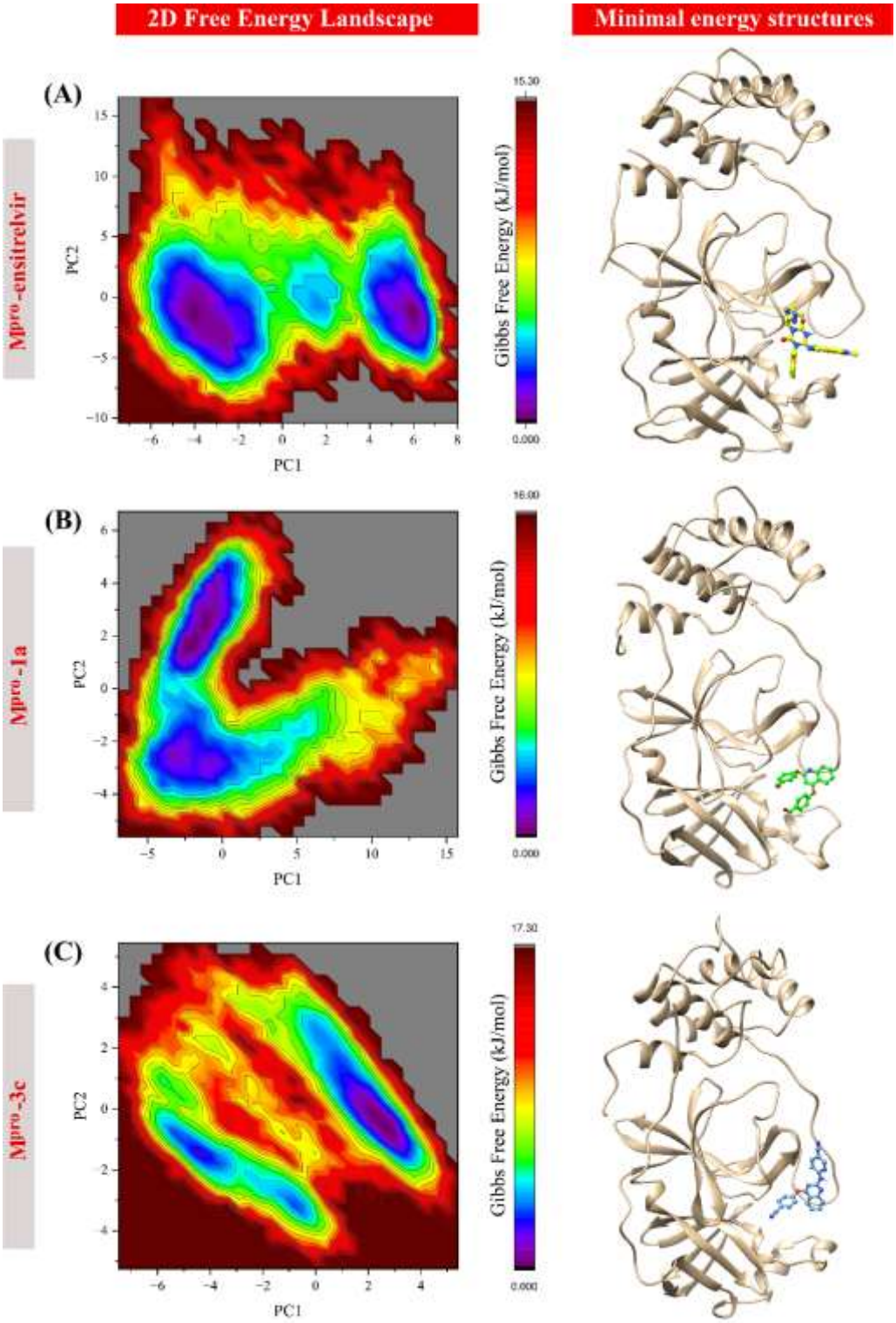


**Figure S5** The Gibbs energy landscapes of (A) $M^{pro}$-nirmatrelvir, (B) $M^{pro}$-**1a**, and (C) $M^{pro}$ -**3c** during a 300 ns MD simulation.

**Table S1** %cells viability and vilucidal activity of quinoline derivatives **1-3(a-d)** and current medications (Ritonavir, Ensitrevir, and Nirmatrelvir).

| Reagents | Concentration (μg/mL) | %Viability | Log Reduction | Efficacy |
|---|---|---|---|---|
| **1a** | 1000 | 47.26±1.94 | - | - |
| | 500 | 73.93±2.20 | 2.890±0.086 | 99.87±0.03 |
| | 250 | 82.62±2.21 | 2.813±0.175 | 99.84±0.07 |
| | 125 | 83.81±1.94 | 2.784±0.105 | 99.83±0.04 |
| | 62.5 | 84.88±0.61 | 2.707±0.125 | 99.80±0.05 |
| | 31.25 | 85.48±0.89 | 2.681±0.088 | 99.77±0.04 |
| | 15.625 | 87.02±1.71 | - | - |
| **1b** | 1000 | 26.67±1.61 | - | - |
| | 500 | 81.67±1.21 | 2.918±0.055 | 99.88±0.02 |
| | 250 | 83.21±1.05 | 2.848±0.139 | 99.85±0.05 |
| | 125 | 84.17±2.07 | 2.828±0.113 | 99.85±0.04 |
| | 62.5 | 84.52±0.84 | 2.771±0.140 | 99.82±0.06 |
| | 31.25 | 86.67±0.89 | 2.763±0.139 | 99.82±0.06 |
| | 15.625 | 88.10±0.61 | - | - |
| **1c** | 1000 | 28.57±1.34 | - | - |
| | 500 | 71.43±1.46 | 3.032±0.156 | 99.90±0.03 |
| | 250 | 76.67±1.10 | 2.911±0.123 | 99.87±0.03 |
| | 125 | 79.76±0.34 | 2.848±0.139 | 99.85±0.05 |
| | 62.5 | 85.48±2.34 | 2.828±0.113 | 99.85±0.04 |
| | 31.25 | 86.79±0.29 | 2.729±0.132 | 99.81±0.06 |
| | 15.625 | 94.64±0.87 | - | - |
| **1d** | 1000 | 67.38±1.02 | - | - |
| | 500 | 83.10±2.11 | 3.063±0.075 | 99.91±0.01 |
| | 250 | 90.12±1.71 | 3.021±0.039 | 99.90±0.01 |
| | 125 | 91.19±1.61 | 2.926±0.050 | 99.88±0.01 |
| | 62.5 | 94.88±1.21 | 2.828±0.113 | 99.85±0.04 |
| | 31.25 | 97.86±1.05 | 2.729±0.132 | 99.81±0.06 |
| | 15.625 | 101.80±1.46 | - | - |
| **2a** | 1000 | 77.38±1.21 | - | - |
| | 500 | 96.98±1.98 | 2.996±0.096 | 99.90±0.02 |
| | 250 | 97.19±3.07 | 2.965±0.043 | 99.89±0.01 |
| | 125 | 97.71±2.45 | 2.848±0.139 | 99.85±0.05 |

| Reagents | Concentration (μg/mL) | %Viability | Log Reduction | Efficacy |
|---|---|---|---|---|
| | 62.5 | 98.75±1.54 | 2.828±0.113 | 99.85±0.04 |
| | 31.25 | 99.79±1.03 | 2.807±0.107 | 99.84±0.04 |
| | 15.625 | 104.38±1.16 | - | - |
| **2b** | 1000 | 54.18±1.78 | - | - |
| | 500 | 93.85±1.45 | 3.078±0.122 | 99.91±0.02 |
| | 250 | 98.23±1.88 | 3.000±0.003 | 99.90±0.00 |
| | 125 | 98.85±1.98 | 3.139±0.107 | 99.93±0.02 |
| | 62.5 | 100.83±0.74 | 2.792±0.103 | 99.83±0.04 |
| | 31.25 | 100.52±1.62 | 2.708±0.103 | 99.80±0.05 |
| | 15.625 | 101.88±1.12 | - | - |
| **2c** | 1000 | 25.71±1.62 | - | - |
| | 500 | 97.24±2.58 | 2.926±0.050 | 99.88±0.01 |
| | 250 | 97.59±2.76 | 2.841±0.140 | 99.85±0.05 |
| | 125 | 98.28±1.38 | 2.820±0.112 | 99.84±0.04 |
| | 62.5 | 98.51±0.86 | 2.707±0.125 | 99.80±0.05 |
| | 31.25 | 99.83±1.90 | 2.686±0.089 | 99.79±0.04 |
| | 15.625 | 102.86±0.77 | - | - |
| **2d** | 1000 | 37.62±0.61 | - | - |
| | 500 | 88.69±1.21 | 2.799±0.104 | 99.84±0.04 |
| | 250 | 95.18±0.54 | 2.707±0.125 | 99.80±0.05 |
| | 125 | 100.00±2.04 | 2.686±0.089 | 99.79±0.04 |
| | 62.5 | 100.71±1.07 | 2.686±0.089 | 99.79±0.04 |
| | 31.25 | 105.36±2.04 | 2.681±0.223 | 99.77±0.09 |
| | 15.625 | 109.17±1.11 | - | - |
| **3a** | 1000 | 36.89±1.10 | - | - |
| | 500 | 95.21±1.56 | 3.346±0.088 | 99.95±0.01 |
| | 250 | 97.60±0.29 | 3.000±0.003 | 99.90±0.00 |
| | 125 | 98.54±0.53 | 2.933±0.049 | 99.88±0.01 |
| | 62.5 | 99.69±1.17 | 2.890±0.086 | 99.87±0.03 |
| | 31.25 | 99.90±1.45 | 2.807±0.107 | 99.84±0.04 |
| | 15.625 | 102.92±1.37 | - | - |
| **3b** | 1000 | 38.56±0.68 | - | - |
| | 500 | 97.43±1.02 | 3.191±0.082 | 99.93±0.01 |
| | 250 | 97.90±1.28 | 3.160±0.075 | 99.93±0.01 |

| Reagents | Concentration (μg/mL) | %Viability | Log Reduction | Efficacy |
|---|---|---|---|---|
| | 125 | 98.67±1.98 | 3.032±0.066 | 99.91±0.01 |
| | 62.5 | 102.19±1.15 | 2.969±0.059 | 99.89±0.02 |
| | 31.25 | 103.33±0.36 | 2.926±0.050 | 99.88±0.01 |
| | 15.625 | 80.10±0.71 | - | - |
| **3c** | 1000 | 25.88±1.77 | - | - |
| | 500 | 81.11±1.81 | 3.782±0.106 | 99.98±0.00 |
| | 250 | 85.44±2.38 | 3.452±0.094 | 99.96±0.01 |
| | 125 | 86.22±0.57 | 3.160±0.073 | 99.93±0.01 |
| | 62.5 | 89.33±0.47 | 3.032±0.066 | 99.91±0.01 |
| | 31.25 | 89.56±0.68 | 2.965±0.043 | 99.89±0.01 |
| | 15.625 | 90.22±1.10 | - | - |
| **3d** | 1000 | 50.11±0.68 | - | - |
| | 500 | 90.22±0.42 | 3.153±0.071 | 99.93±0.01 |
| | 250 | 91.22±1.85 | 3.063±0.075 | 99.91±0.01 |
| | 125 | 92.67±1.19 | 3.032±0.066 | 99.91±0.01 |
| | 62.5 | 92.89±1.13 | 3.011±0.186 | 99.90±0.04 |
| | 31.25 | 94.89±1.93 | 3.000±0.003 | 99.90±0.00 |
| | 15.625 | 97.44±1.75 | - | - |
| Ritonavir | 1000 | 21.14±0.62 | - | - |
| | 500 | 27.05±0.82 | - | - |
| | 250 | 54.95±0.82 | - | - |
| | 125 | 71.71±1.82 | 3.578±0.084 | 99.97±0.01 |
| | 62.5 | 73.52±1.85 | 3.503±0.121 | 99.97±0.01 |
| | 31.25 | 75.71±1.15 | 3.284±0.038 | 99.95±0.00 |
| | 15.625 | 76.10±0.49 | 3.246±0.074 | 99.94±0.01 |
| | 7.813 | 76.86±2.57 | 3.153±0.037 | 99.93±0.01 |
| Ensitrevir | 1000 | 24.76±1.32 | - | - |
| | 500 | 54.00±0.84 | - | - |
| | 250 | 80.19±1.64 | 3.261±0.050 | 99.94±0.01 |
| | 125 | 81.05±0.94 | 3.106±0.083 | 99.92±0.02 |
| | 62.5 | 85.62±2.78 | 3.000±0.067 | 99.90±0.02 |
| | 31.25 | 87.33±0.59 | 3.021±0.107 | 99.90±0.03 |
| | 15.625 | 89.33±1.17 | 3.000±0.100 | 99.90±0.02 |
| Nirmatrelvir | 1000 | 55.81±1.10 | - | - |

| Reagents | Concentration (μg/mL) | %Viability | Log Reduction | Efficacy |
|---|---|---|---|---|
| | 500 | 73.51±1.28 | 3.153±0.037 | 99.93±0.01 |
| | 250 | 75.25±1.55 | 3.021±0.039 | 99.90±0.01 |
| | 125 | 77.15±0.84 | 3.011±0.186 | 99.90±0.04 |
| | 62.5 | 78.18±1.55 | 3.000±0.003 | 99.90±0.00 |
| | 31.25 | 80.65±1.63 | 2.828±0.113 | 99.85±0.04 |
| | 15.625 | 82.86±1.07 | - | - |
| Paxlovid (Ritonavir/ Nirmatrelvir ; 1:3) | 1000 | 42.28± 1.68 | - | - |
| | 500 | 80.10± 0.71 | 3.191±0.082 | 99.93±0.01 |
| | 250 | 83.14± 1.20 | 3.000±0.100 | 99.90±0.02 |
| | 125 | 85.81± 1.55 | 2.990±0.082 | 99.90±0.02 |
| | 62.5 | 86.76±0.84 | 2.990 ±0.082 | 99.90±0.02 |
| | 31.25 | 92.76±1.64 | 2.905±0.082 | 99.87±0.03 |
| | 15.625 | 92.76±1.64 | - | - |

[a]Results are expressed as mean±SD of quadruplicate experiments.

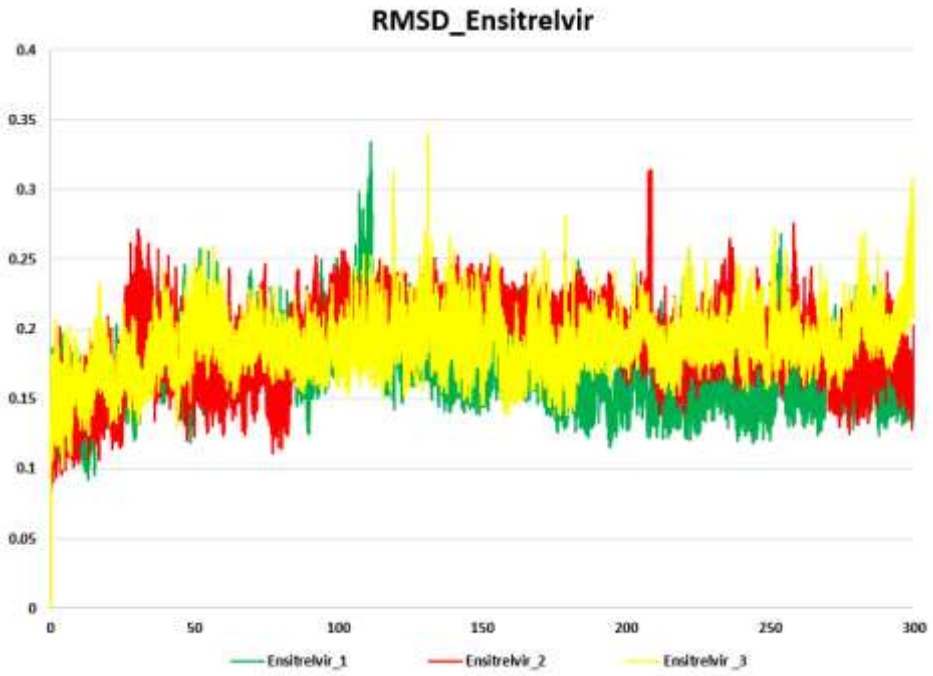


**Figure S6** RMSD analysis of MD simulation triplicates of the $M^{pro}$- ensitrelvir complex over 300 ns.

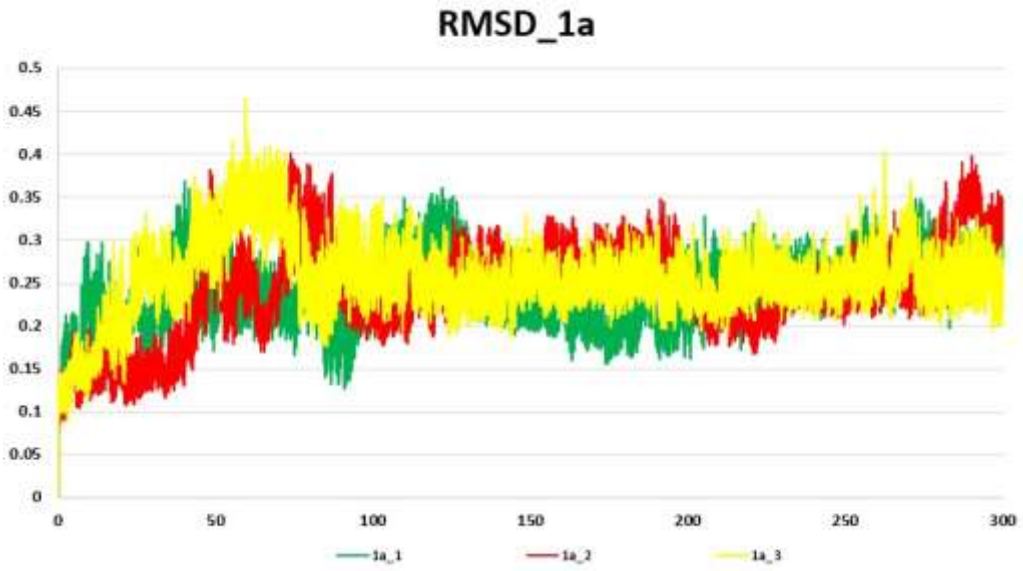


**Figure S7** RMSD analysis of MD simulation triplicates of the M$^{pro}$-**1a** complex over 300 ns.

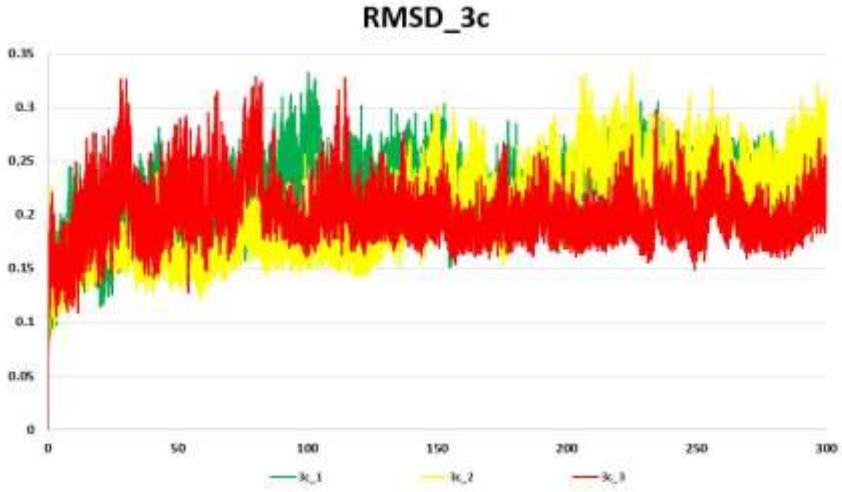


**Figure S8** RMSD analysis of MD simulation triplicates of the M$^{pro}$-**3c** complex over 300 ns.

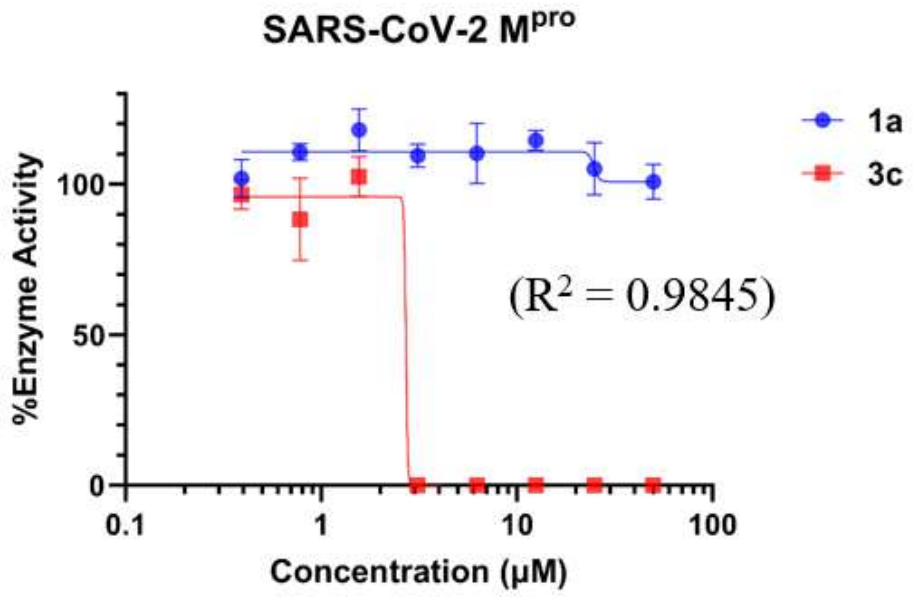


**Figure S9** Dose-dependent curve of 1a and 3c against SARS-CoV-2 $M^{pro}$ ($R^2$ = 0.9845).

**Table S2** Binding energies and individual component energy values obtained from the MM-GBSA and MM-PBSA calculation of $M^{pro}$- nirmatrelvir, $M^{pro}$-ensitrelvir, $M^{pro}$-**1a** and $M^{pro}$-**3c** complexes.

| Energetic terms (kcal/mol) | 1a | 3c | Ensitrelvir | Nirmatrelvir |
|---|---|---|---|---|
| $\Delta E_{vdw}$ | -37.99±2.56 | -40.06±2.94 | -50.50±3.59 | -52.11±3.08 |
| $\Delta E_{ele}$ | -2.24±2.56 | -3.49±0.93 | -8.57±1.58 | -13.28±1.54 |
| $\Delta G_{polar/GB}$ | 7.44±0.87 | 7.57±0.14 | 14.78±1.29 | 18.87±1.14 |
| $\Delta G_{non\text{-}polar/GB}$ | -4.61±0.28 | -4.88±0.44 | -5.76±0.33 | -6.32±0.27 |
| $\Delta G_{polar/PB}$ | 8.20±0.86 | 8.19±1.02 | 15.62±1.57 | 19.38±1.24 |
| $\Delta G_{non\text{-}polar/PB}$ | -3.34±0.13 | -3.69±0.20 | -4.50±0.29 | -4.49±0.14 |
| $-T\Delta S$ | 6.90±0.14 | 6.54±0.13 | 9.89±0.13 | 6.12±0.34 |
| $\Delta G_{bind/GB}$ | -30.51±2.56 | -34.32±3.14 | -40.16±4.81 | -48.74±2.85 |
| $\Delta G_{bind/PB}$ | -28.47±2.45 | -32.51±2.86 | -38.05±4.70 | -46.40±2.75 |

$\Delta E_{vdw}$ = van der Waals energy, $\Delta E_{elec}$ = electrostatic energy, $\Delta G_{polar/GB}$ = The polar solvation free energy obtained from the generalized Born method, $\Delta G_{non\text{-}polar/}$GB = Nonpolar solvation free energy obtained from the generalized Born method, $\Delta G_{polar/PB}$ = The polar solvation free energy obtained from the Poisson-Boltzmann method, $\Delta G_{non\text{-}polar/PB}$ = Nonpolar solvation energy obtained from the Poisson-Boltzmann method, $-T\Delta S$ = Interaction entropy, $\Delta G_{Binding/GB}$ = Binding free energy (kcal/mol) from the generalized Born method, $\Delta G_{Binding/PB}$ = Binding free energy (kcal/mol) from the Poisson-Boltzmann method.

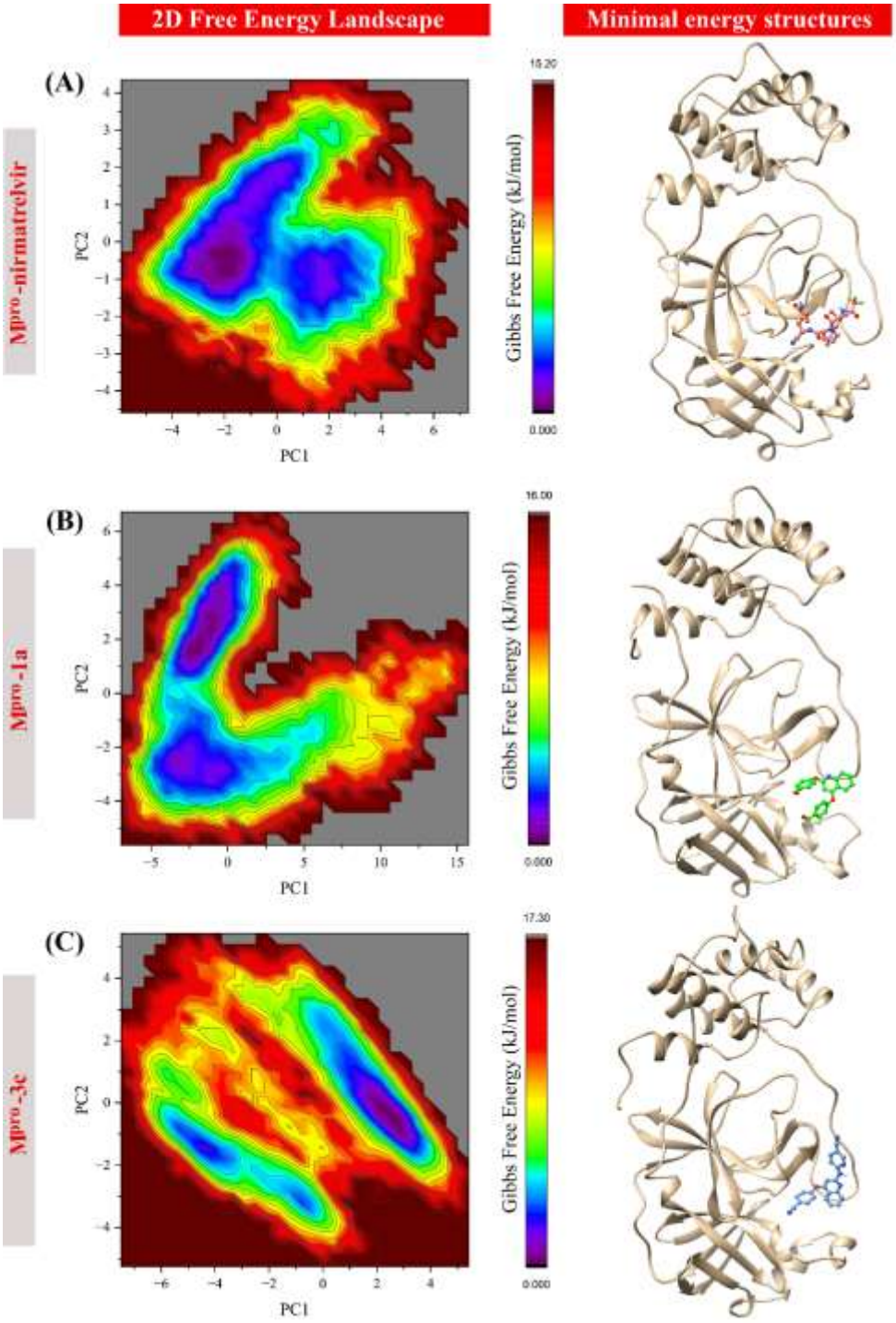


**Figure S10** The Gibbs energy landscapes of (A) $M^{pro}$-nirmatrelvir, (B) $M^{pro}$-**1a**, and (C) $M^{pro}$ -**3c** during a 300 ns MD simulation.

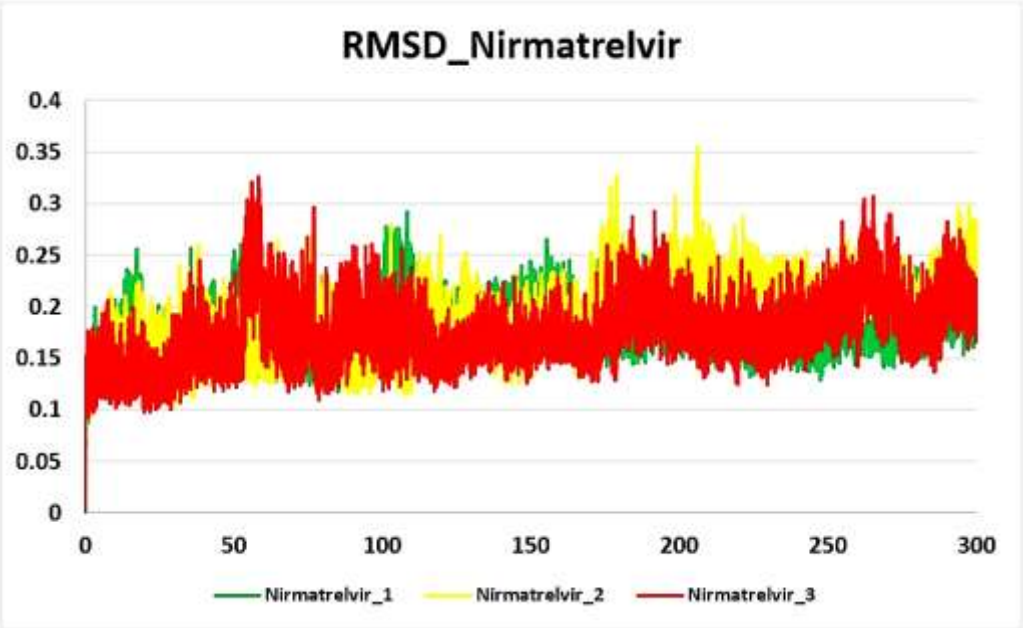


**Figure S11** RMSD analysis of MD simulation triplicates of the $M^{pro}$-nirmatrelvir complex over 300 ns.